



# Solar photocatalytic degradation of emerging contaminants using NH<sub>2</sub>-MIL-125 grafted by heterocycles

V. Muelas-Ramos, M. Peñas-Garzón, J.J. Rodríguez, J. Bedia<sup>\*</sup>, C. Belver<sup>\*</sup>

Chemical Engineering Department, Universidad Autónoma de Madrid, Campus Cantoblanco, E-28049 Madrid, Spain

## ARTICLE INFO

### Keywords:

NH<sub>2</sub>-MIL-125

Grafting

Emerging contaminants

Solar photocatalysis

Continuous regime

## ABSTRACT

This work reports the photocatalytic performance of NH<sub>2</sub>-MIL-125 grafted by heterocycles for the removal of contaminants of emerging concern under solar light. Grafting NH<sub>2</sub>-MIL-125 with different heterocyclic carboxaldehydes reduces the band gap, thanks to the performance of the heterocycle as an antenna for light absorption. Grafting with 3-pyridinecarboxaldehyde (3PA) results in the best light harvesting for the degradation of acetaminophen in different water matrices. The abatement of additional emerging contaminants, i.e., antipyrine and sulfamethoxazole, was also evaluated. The photocatalytic performance depends on the nature of the target compound. Trapping experiments conclude that superoxide radicals are the main reactive species involved in the photodegradation process, while electrons and hydroxyl radicals play a minor role. The 3PA-grafted photocatalyst shows remarkable constant performance in a novel analysis in a continuous flow regime, achieving total conversion of acetaminophen (ACE) for 16 h on stream. The results herein described provide a comprehensive insight into the solar photocatalytic degradation of emerging contaminants using NH<sub>2</sub>-MIL-125 grafted by aromatic heterocycles.

## 1. Introduction

The uncontrolled discharge of different compounds into aquatic sources constitutes an increasing concern. Pharmaceuticals are common emerging contaminants (ECs) detected in wastewaters and aquatic ecosystems, coming from household effluents, industrial activities, and hospital services, among others [1]. Exposure to ECs may produce harmful effects on human health and the environment, such as disruptive effects or cellular damage [2,3]. Water streams containing ECs are mixed with other water flows and treated into wastewater treatment plants (WWTPs) before final discharge into rivers, seas, or aquifers. However, the development of more accurate analytical techniques has allowed the detection of ECs in the WWTPs effluents, confirming that they are not completely removed during the process [4]. In this sense, the average removal of analgesics, anti-inflammatories, or  $\beta$ -blockers was estimated to be around 30–40% [5]. Acetaminophen (ACE) can be considered among the most common analgesic-antipyretic pharmaceuticals worldwide, also sold under different trade names, such as paracetamol. The consumption of ACE is situated among 60–70 daily doses per 1000 inhabitants (DDD) in European countries such as France, Spain, Denmark, and the United Kingdom, much higher than that of

other common analgesics, such as acetylsalicylic acid, with a reported consumption below 10 DDD [6]. After consumption, about 2–5% of ACE is excreted without any metabolic shift and reaches wastewater [7]. Its high solubility in water (around 14 g·L<sup>-1</sup> besides the low octanol-water partition coefficient, 0.46 [8]) can explain its common detection in water bodies. For instance, Fekadu et al. [9] compared the occurrence of certain pharmaceuticals in European and African freshwater aquatic environments. They found that the maximum ACE concentration recorded in Europe was in the Llobregat river (Spain), with a value of 1.3  $\mu\text{g}\cdot\text{L}^{-1}$  [10], remarkably lower than the measured in a Kenyan river, 107  $\mu\text{g}\cdot\text{L}^{-1}$  [11]. The incomplete elimination of these emerging contaminants would increase their overall concentration, thus representing a potential environmental risk. Therefore, it is necessary to improve strategies in the treatment of wastewaters for the complete removal of these ECs before their final discharge. For instance, advanced oxidation processes (AOPs) are based on the in-situ generation of reactive oxygen species (ROS) with high oxidation capacity [12,13], including Fenton-like processes, ozonation, electrochemical oxidation, or photocatalysis [14]. Particularly, photocatalysis, based on the conversion of light-to-chemical energy, is considered an environmentally friendly technology because it only requires the use of a light source and a solid

<sup>\*</sup> Corresponding authors.

E-mail addresses: [jorge.bedia@uam.es](mailto:jorge.bedia@uam.es) (J. Bedia), [carolina.belver@uam.es](mailto:carolina.belver@uam.es) (C. Belver).

<https://doi.org/10.1016/j.seppur.2022.121442>

Received 16 March 2022; Received in revised form 4 June 2022; Accepted 5 June 2022

Available online 7 June 2022

1383-5866/© 2022 The Authors. Published by Elsevier B.V. This is an open access article under the CC BY-NC-ND license (<http://creativecommons.org/licenses/by-nc-nd/4.0/>).

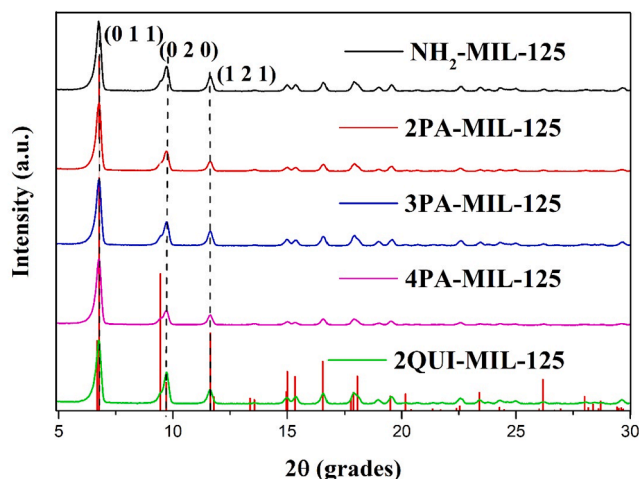


**Fig. 1.** X-ray diffraction patterns of the bare  $\text{NH}_2$ -MIL-125 and the grafted materials (Reference pattern of  $\text{NH}_2$ -MIL-125 from Crystal Open Database (COD) library is included in red colour). (For interpretation of the coloured references in this figure legend, the reader is referred to the web version of this article.)

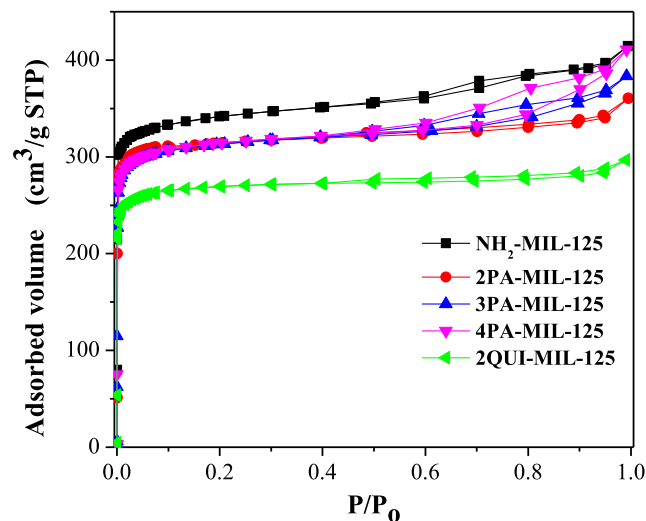


**Fig. 3.**  $\text{N}_2$  adsorption-desorption isotherms at 196 °C of the bare  $\text{NH}_2$ -MIL-125 and the grafted materials.

**Table 1**

Porous texture parameters and band gap values ( $E_g$ ) of the bare  $\text{NH}_2$ -MIL-125 and the grafted materials.

	$S_{\text{BET}}$ ( $\text{m}^2\cdot\text{g}^{-1}$ )	$S_{\text{MP}}$ ( $\text{m}^2\cdot\text{g}^{-1}$ )	$S_{\text{EXT}}$ ( $\text{m}^2\cdot\text{g}^{-1}$ )	$V_{\text{MP}}$ ( $\text{cm}^3\cdot\text{g}^{-1}$ )	$V_{\text{T}}$ ( $\text{cm}^3\cdot\text{g}^{-1}$ )	$E_g$ (eV)
$\text{NH}_2$ -MIL-125	1141	985	157	0.46	0.64	2.67
2PA-MIL-125	1032	918	114	0.43	0.58	2.63
3PA-MIL-125	1053	927	126	0.43	0.59	2.62
4PA-MIL-125	1062	937	126	0.43	0.63	2.60
2QUI-MIL-125	911	840	72	0.38	0.46	2.60

$S_{\text{BET}}$ , specific surface area;  $S_{\text{MP}}$  and  $S_{\text{EXT}}$ , microporous and non-microporous surface area;  $V_{\text{T}}$  and  $V_{\text{MP}}$ , total and micropore volume;  $E_g$ , band gap.

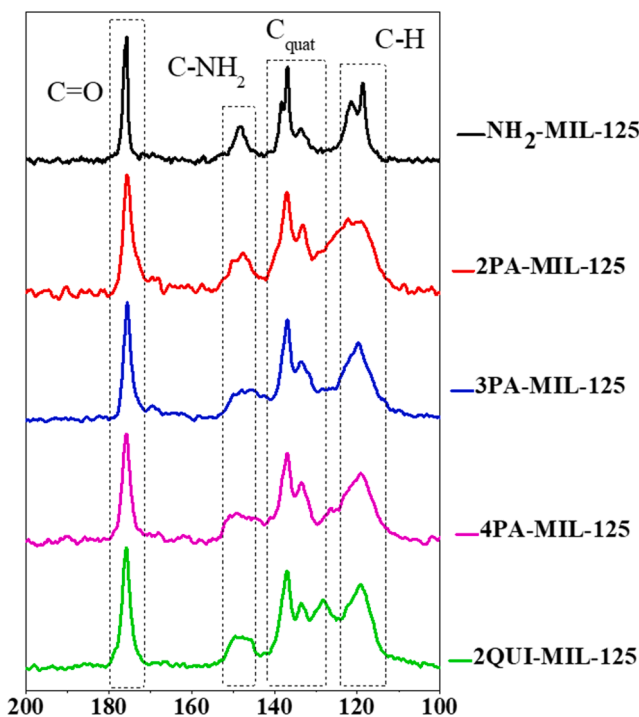


**Fig. 2.**  $^{13}\text{C}$  solid-state NMR spectra of the bare  $\text{NH}_2$ -MIL-125 and the grafted materials.

semiconductor, and can operate under mild conditions of temperature and pressure. Moreover, the use of solar light represents a cost-effective and green alternative to other more energy-demand technologies, supporting the development of photocatalysis for the abatement of contaminants in water. Thus, the removal of ECs by solar photocatalysis is the focus of many researchers, with particular emphasis on the degradation of analgesics [15–19] and antibiotics [20–22].

Since the photocatalytic process requires the absorption of light by a semiconductor, many different materials are currently under study to achieve the best solar light harvesting [23]. The main aim in this field is the absorption of light in both the UV and visible range of the solar spectrum to generate electron/hole pairs while avoiding their

recombination [24]. Despite the adequate activity reported using  $\text{TiO}_2$  as a reference photocatalyst [25], this semiconductor presents the main limitation of its large band gap value ( $\sim 3.2$  eV), avoiding the light-harvesting from the visible region and thus implying a low utilization of the solar light. In this sense, metal organic frameworks (MOFs) are being investigated for the photocatalytic treatment of contaminated water [26,27], as a consequence of their good optical, structural, and electronic properties that can be tailored through the use of different metal nodes or organic linkers [28]. After irradiation, electrons can be transferred from the organic ligand to the partially filled d-orbitals of the metal cluster in a process known as ligand-to-metal charge transfer (LMCT) [29,30]. Among the most used MOFs are Fe-based (as MIL-53, -88, and -101), Ti-MOFs (MIL-125), Zr-MOFs (UiO-66), and Zn-MOFs (ZIF-8) [31]. Moreover, the literature shows additional strategies to promote the photocatalytic performance of MOFs to enhance their light harvesting, such as doping [32], noble metal deposition [33], or combined with other semiconductors [34]. One approach consists in functionalizing the organic ligand [35]. For example,  $\text{NH}_2$ -MIL-125 has shown high stability [36] and activity concerning the bare MIL-125 counterpart, as both the  $\text{NH}_2$ -ligand and the Ti-cluster were excited under visible light [37]. This approach can be further extended by grafting, after synthesis, the  $-\text{NH}_2$  group with other compounds that act

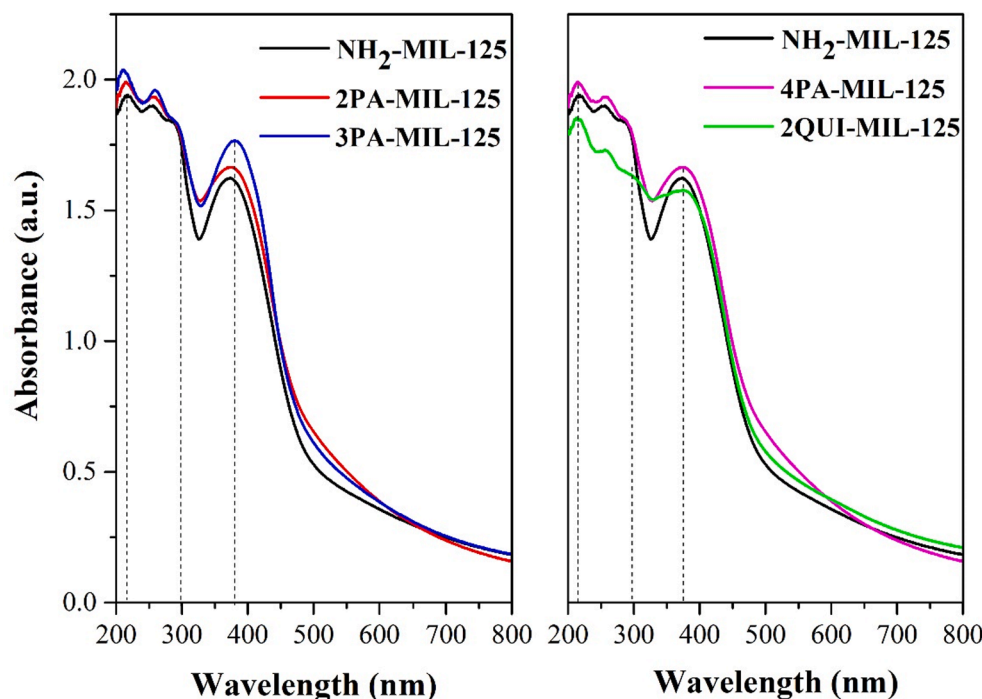


Fig. 4. UV-visible spectra of the bare  $\text{NH}_2\text{-MIL-125}$  and the grafted materials.

as an antenna for light absorption [38]. In this sense, heterocyclic compounds can be successfully grafted to the  $\text{-NH}_2$  group following a Schiff base reaction through an aldehyde group [39]. These heterocyclic compounds provide additional charges and improve their mobility, appearing as a promising approach to improving the photocatalytic properties of MOFs [40]. However, to the best of our knowledge, no studies have been reported dealing with the grafting of MOFs for the solar photocatalytic degradation of ECs.

This is the first work reporting the degradation of ECs for water purification using these grafted- $\text{NH}_2\text{-MIL-125}$ . The grafted-MOFs were tested in the photodegradation of ACE. The photocatalytic performance of the best grafted- $\text{NH}_2\text{-MIL-125}$  was further investigated under different water matrices and with a mixture of emerging contaminants (acetaminophen, sulfamethoxazole, and antipyrine) whose presence in aqueous effluents has been also frequently reported [41]. Besides, the stability and photocatalytic performance were evaluated under a novel analysis in continuous flow tests. Remarkably, no previous works have demonstrated the performance of grafted- $\text{NH}_2\text{-MIL-125}$  in continuous flow tests or with a mixture of emerging contaminants with different chemical structures.

## 2. Experimental

### 2.1. Chemicals and reagents

2-aminoterephthalic acid (ATA, 99%), N,N-dimethylformamide (DMF,  $\geq 99.8\%$ ), titanium (IV) isopropoxide ( $\geq 97\%$ ), methanol (99.8%), 2-pyridinecarboxaldehyde (2PA, 99%), 3-pyridinecarboxaldehyde (3PA, 98%), 4-pyridinecarboxaldehyde (4PA, 97%), 2-quinolinecarboxaldehyde (2QUI, 97%), acetaminophen (ACE,  $\geq 99\%$ ), sulfamethoxazole (SMX,  $\geq 99\%$ ), antipyrine (ANT,  $\geq 99\%$ ), acetic acid ( $\geq 99\%$ ), benzoquinone (BQ  $\geq 98\%$ ), silver nitrate, ( $\text{AgNO}_3$ ,  $\geq 99\%$ ), potassium iodide (KI, 99%) and  $\text{NaHCO}_3$  were purchased from Sigma-Aldrich. Acetonitrile (UV HPLC grade) and  $\text{Na}_2\text{SO}_4$  ( $\geq 99\%$ ) were acquired from Scharlab. 2-propanol (IPA, 99.7%) was acquired from AppliChem, whereas NaCl and  $\text{NaNO}_3$  were provided from Panreac. All chemicals were used as received without further purification. All solutions were prepared with deionized water (type II).

### 2.2. Synthesis of bare $\text{NH}_2\text{-MIL-125}$

The  $\text{NH}_2\text{-MIL-125}$  was synthesized by solvothermal synthesis following a previously described method [36]. Briefly, 6 mmol of 2-aminoterephthalic acid were dissolved in 25 ml of DMF and stirred for 5 min at 25 °C. Then, 3 mmol of titanium (IV) isopropoxide were added dropwise, followed by the addition of 25 ml of methanol. After 30 min of stirring, the mixture was placed in a 100 ml Teflon steel autoclave and heated for 16 h at 150 °C. The resulting yellow powder was recovered by centrifugation (5000 rpm, 5 min) and washed with DMF and methanol (100 ml each time for 30 min). The product was finally dried in an oven at 60 °C for 18 h.

### 2.3. Grafting of $\text{NH}_2\text{-MIL-125}$

The  $\text{NH}_2\text{-MIL-125}$  was modified after synthesis by grafting with four heterocyclic carboxaldehydes, namely 2-pyridinecarboxaldehyde, 3-pyridinecarboxaldehyde, 4-pyridinecarboxaldehyde, and 2-quinolinecarboxaldehyde, whose chemical structures can be seen in Fig. S1. The grafting process followed the method described by Wu et al. [38]. It consists of the Schiff reaction between the amine group of the MOF and the carboxylic group of the heterocyclic carboxaldehyde, as schematized in Fig. S2. Briefly, 560 mg of  $\text{NH}_2\text{-MIL-125}$  was firstly activated in a vacuum oven at 120 °C for 3 h. Then, it was dispersed in 30 ml of acetonitrile, followed by the addition of 0.8 mM of 2PA. The mixture was placed in a bath at 70 °C for three days. The resulting solid was collected by centrifugation (5000 rpm and 5 min), washed with methanol three times, and dried at 60 °C for 18 h in a vacuum oven. For complete removal of organic precursors and solvent, the solid was heated in air at 200 °C for 48 h. The material thus obtained was named 2PA-MIL-125, according to the abbreviation of the heterocyclic carboxaldehyde. The  $\text{NH}_2\text{-MIL-125}$  was grafted by the other heterocyclic carboxaldehydes, 3PA, 4PA, and 2QUI, following the same methodology, and the resulting materials were labelled as 3PA-MIL-125, 4PA-MIL-125, and 2QUI-MIL-125, respectively.

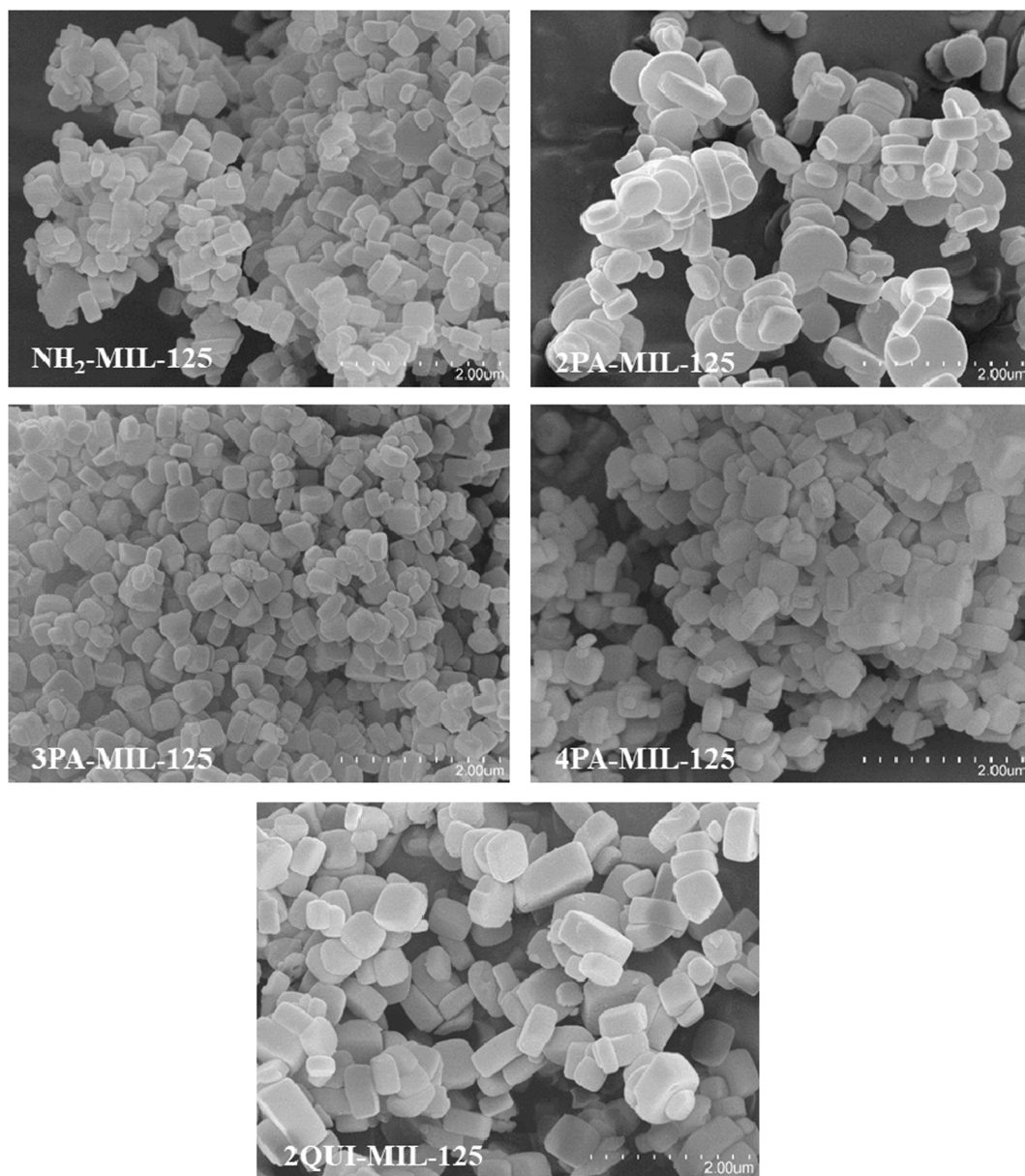


Fig. 5. SEM images of the bare  $\text{NH}_2$ -MIL-125 and the grafted materials.

#### 2.4. Characterization of photocatalysts

A Bruker D8 diffractometer (Cu  $\text{K}\alpha$  source) in a  $2\theta$  scanning range of 2 to  $50^\circ$  and with a  $5^\circ\cdot\text{min}^{-1}$  rate, was used to record the X-ray diffraction (XRD) patterns. The  $^{13}\text{C}$  solid-state NMR spectra were acquired with a Bruker AV 400 WB spectrometer at 100.61 MHz in ZrO rotors sealed with Kel-F caps at room temperature. The analysis conditions were contact time 3 ms, spinning frequency 10 kHz, and pulse delay 4 s. Chemical shifts were all reported concerning external tetramethylsilane (TMS). The porous texture was characterized by  $\text{N}_2$  adsorption-desorption at  $-196^\circ\text{C}$  performed with a TriStar 123 equipment (Micromeritics). All photocatalysts were previously outgassed under vacuum at  $120^\circ\text{C}$ . The specific surface area ( $S_{\text{BET}}$ ) was obtained from the BET method [42], while the microporous surface area ( $S_{\text{MP}}$ ) and the non-microporous surface area ( $S_{\text{EXT}}$ ) were quantified by the t-plot [43]. The amount of nitrogen adsorbed at a relative pressure ( $P/P_0$ ) of 0.99 was used to estimate the total pore volume. UV-vis diffuse reflectance spectra were collected in a Shimadzu 2600 UV-vis spectrophotometer in the 185–800 nm range, using  $\text{BaSO}_4$  as reference. The

band gap ( $E_g$ ) values were determined by the Tauc Plot method [35,44], considering all materials as indirect semiconductors [45]. Scanning electron microscopy (SEM) images were acquired with HITACHI S-4800 equipment. Photoluminescence (PL) spectra were recorded in a Cary Eclipse spectrofluorometer using an excitation wavelength of 370 nm. A Metrohm Autolab potentiostat (PGSTAT204) was used to determine the electrochemical properties of the synthesized materials. This system comprises an indium tin oxide (ITO) working electrode, with counter and reference counterparts of carbon and silver electrodes, respectively. The material suspension ( $1\text{ mg}\cdot\text{mL}^{-1}$ ) was prepared in 0.1 M  $\text{Na}_2\text{SO}_4$  ( $\text{pH} \sim 4.3$  at  $25^\circ\text{C}$ ) and placed into the electrochemical cell (DropSens ITO10). Electrochemical impedance spectroscopy (EIS) was recorded scanning the frequency range from  $10^5$  to  $10^{-1}$  Hz at a fixed potential of  $-1.2\text{ V}$ , whereas Mott-Schottky plots were obtained applying a voltage between 0.4 and  $-1.0\text{ V}$  under a constant frequency of 100 Hz. The flat band potential of the material,  $V_{\text{fb}}$ , was obtained following Mott-Schottky equation (Eq. (1)) [46]:



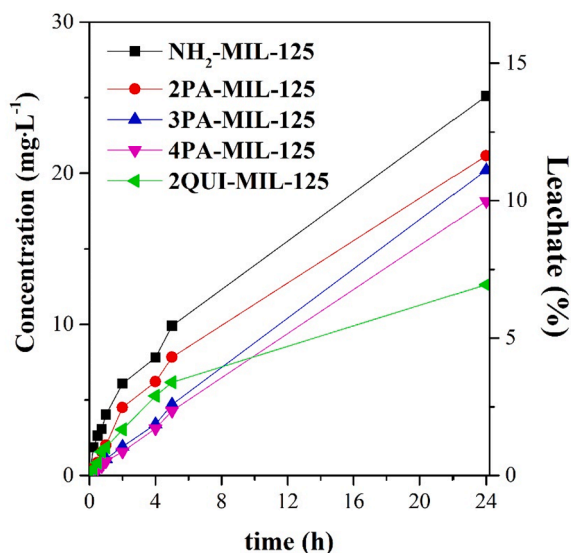


Fig. 6. Evolution of the linker leaching in the water of the bare  $\text{NH}_2\text{-MIL-125}$  and the grafted materials.

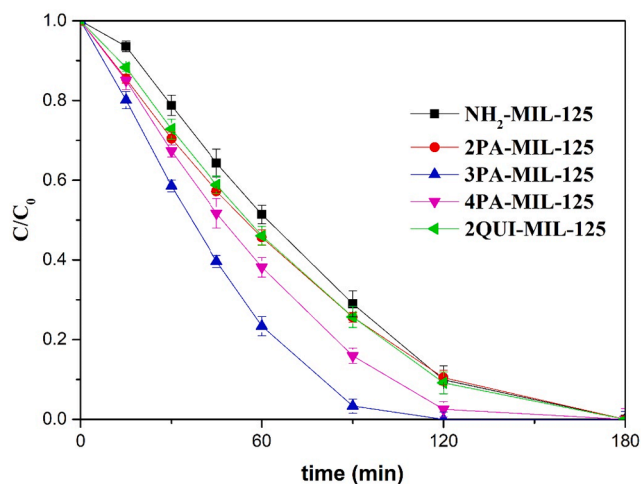


Fig. 7. Evolution of ACE degradation with the bare  $\text{NH}_2\text{-MIL-125}$  and the grafted materials under solar irradiation ( $[\text{ACE}]_0 = 5 \text{ mg}\cdot\text{L}^{-1}$ ; Photocatalyst load =  $250 \text{ mg}\cdot\text{L}^{-1}$ ; Intensity =  $600 \text{ W}\cdot\text{m}^{-2}$ ).

Table 2

Values of the pseudo-first-order rate constant ( $k$ ) of ACE degradation under solar irradiation.

Photocatalyst	$k \text{ (min}^{-1}\text{)}$	Reference
$\text{NH}_2\text{-MIL-125}$	0.0082	This work
2PA-MIL-125	0.0126	This work
3PA-MIL-125	0.0194	This work
4PA-MIL-125	0.0151	This work
2QUI-MIL-125	0.0137	This work
Zr-doped $\text{NH}_2\text{-MIL-125}$	0.0121	[32]
Pt@ $\text{NH}_2\text{-MIL-125}$	0.0165	[33]

$$\frac{1}{C^2} = \frac{2}{\varepsilon \hat{A} \cdot \varepsilon_0 \hat{A} \cdot e \hat{A} \cdot N_D} \hat{A} \cdot \left( V - V_{fb} - \frac{k \hat{A} \cdot T}{e} \right) \xrightarrow{1/C^2=0} V_{fb} = V - \frac{k \hat{A} \cdot T}{e} \quad (1)$$

being  $C$  the capacitance of the semiconductor-electrolyte junction at applied voltage  $V$ ;  $\varepsilon$  and  $\varepsilon_0$  the permittivity of the semiconductor and the void, respectively;  $e$  the electron charge ( $1.602 \cdot 10^{-19} \text{ J}$ );  $k$  the

Boltzmann's constant ( $8.617 \cdot 10^{-5} \text{ eV}\cdot\text{K}^{-1}$ ); and  $T$  the temperature (298 K).  $V_{fb}$  is estimated from the intercept point of the tangent line with the potential axis ( $1/C^2 = 0$ ) in the plot of  $1/C^2$  vs  $V$ . The potential of the conduction band ( $V_{CB}$ ) can be calculated concerning the normal hydrogen electrode (NHE) at pH 7 following a Nernstian shift using Eq. (2) [47]:

$$V_{CB} = V_{fb(\text{Ag/AgCl,pH})} + \Delta V_{(\text{Ag/AgCl,NHE})} - 0.059 \cdot (7 - \text{pH}), \quad (2)$$

where  $\Delta V_{(\text{Ag/AgCl,NHE})}$  is the Ag/AgCl potential against NHE (0.21 V). Finally, the valence band potential ( $V_{VB}$ ) can be estimated following Eq. (3):

$$V_{VB} = V_{CB} + \frac{E_g}{e}, \quad (3)$$

where  $E_g$  is the bandgap of the semiconductor.

## 2.5. Photocatalytic assays

Photocatalytic assays were performed in a Pyrex jacketed reactor under simulated solar light (Suntest XLS+, Xe lamp, ATLAS). The light intensity was fixed at  $600 \text{ W}\cdot\text{m}^{-2}$  and restrained to  $\lambda \geq 320 \text{ nm}$  with an ID65 filter. An aqueous solution (150 ml) of the target contaminant was placed in the reactor with the photocatalyst ( $250 \text{ mg}\cdot\text{L}^{-1}$ ) under stirring, setting the temperature at  $25^\circ\text{C}$ . For all assays, the initial concentration of the target compound was set at  $5 \text{ mg}\cdot\text{L}^{-1}$  after reaching the adsorption equilibrium in the dark. Aliquots of  $400 \mu\text{L}$  were taken during reaction at different intervals, filtered with PTFE syringeless filters (Whatman 0.45  $\mu\text{m}$ ) and analysed by High Performance Liquid Chromatography (HPLC), using a reverse phase C18 column. The mobile phase used was a mixture of acetic acid 0.1% (v/v) and acetonitrile using a gradient elution method (10/90 to 40/60%), with a constant flow equal to  $0.7 \text{ ml}\cdot\text{min}^{-1}$  for the identification of ACE and ANT, while SMX was determined by an isocratic 70/30% method. The detection wavelength was fixed at the maximum absorption of each target contaminant, i.e., 246, 254, and 242 nm for ACE, SMX, and ANT, respectively. The possible lixiviation of the organic linker of the MOFs was also monitored by using the same chromatographic method, setting the detection wavelength at 358 nm. The photodegradation of a mixture of these three pharmaceuticals was evaluated using the material with the best performance, setting the initial concentration of each contaminant at  $5 \text{ mg}\cdot\text{L}^{-1}$  after adsorption under the same conditions previously described. Radical trapping experiments were carried out with p-benzoquinone (BQ) as a scavenger for superoxide radicals ( $\text{O}_2^{\cdot-}$ ), isopropanol (IPA) for hydroxyl radicals ( $\text{HO}^{\cdot}$ ), silver nitrate for electrons ( $e^-$ ), and potassium iodide (KI) as hole quenchers ( $h^+$ ). These experiments were performed under the same conditions as the reaction ones, adding the scavenger at 1 mM initial concentration to the ACE solution after the dark adsorption equilibrium step [33]. The photocatalytic performance was also investigated in different water matrices. Specifically, tap water and synthetic water with  $\text{Cl}^-$  ( $25 \text{ mg}\cdot\text{L}^{-1}$ ),  $\text{NO}_3^-$  ( $50 \text{ mg}\cdot\text{L}^{-1}$ ),  $\text{SO}_4^{2-}$  ( $50 \text{ mg}\cdot\text{L}^{-1}$ ), and  $\text{HCO}_3^-$  ( $150 \text{ mg}\cdot\text{L}^{-1}$ ) as usual concentrations of these ions in real water samples [33]. Tests were carried out in triplicate and the average value was included. A continuous experiment was carried out in the experimental setup schematized in Fig. S3, coupling an inlet and outlet flow by two different pumps at  $0.9 \text{ ml}\cdot\text{min}^{-1}$ . A filter was placed in the outlet pipe to avoid photocatalyst loss. After the reaction, the photocatalyst was recovered by filtration (PTFE, Whatman 0.45  $\mu\text{m}$ ), washed three times with 300 ml of water, and dried at  $60^\circ\text{C}$  overnight. This used photocatalyst was characterized by X-ray diffraction and  $\text{N}_2$  adsorption-desorption ( $-196^\circ\text{C}$ ). The quantification of short-chain carboxylic acids was performed using a Supelcogel C-610H column. The mobile phase consisted of an isocratic 0.1%  $\text{H}_3\text{PO}_4$  solution at a flow rate of  $0.5 \text{ ml}\cdot\text{min}^{-1}$  ( $30^\circ\text{C}$ ), fixing the excitation wavelength at 210 nm. The corresponding standard solutions were used to identify the carboxylic acids.

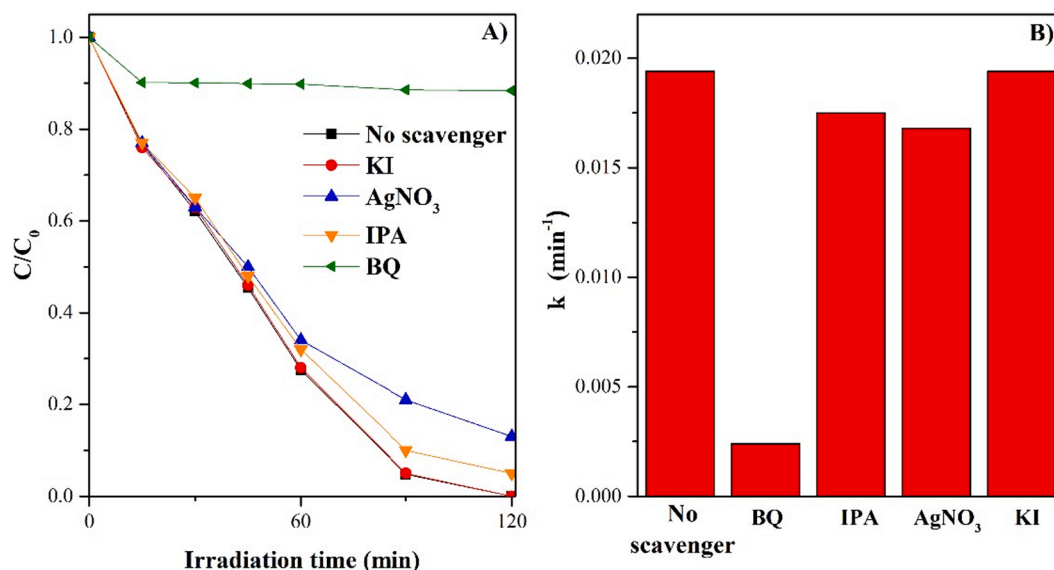


**Fig. 8.** A) ACE evolution in presence of different scavengers, and B) corresponding pseudo-first-order rate under solar light using 3PA-MIL-125 ( $[\text{ACE}]_0 = 5 \text{ mg}\cdot\text{L}^{-1}$ ;  $[\text{scavenger}] = 1 \text{ mM}$ ; Photocatalyst load =  $250 \text{ mg}\cdot\text{L}^{-1}$ ; Intensity =  $600 \text{ W}\cdot\text{m}^{-2}$ ).

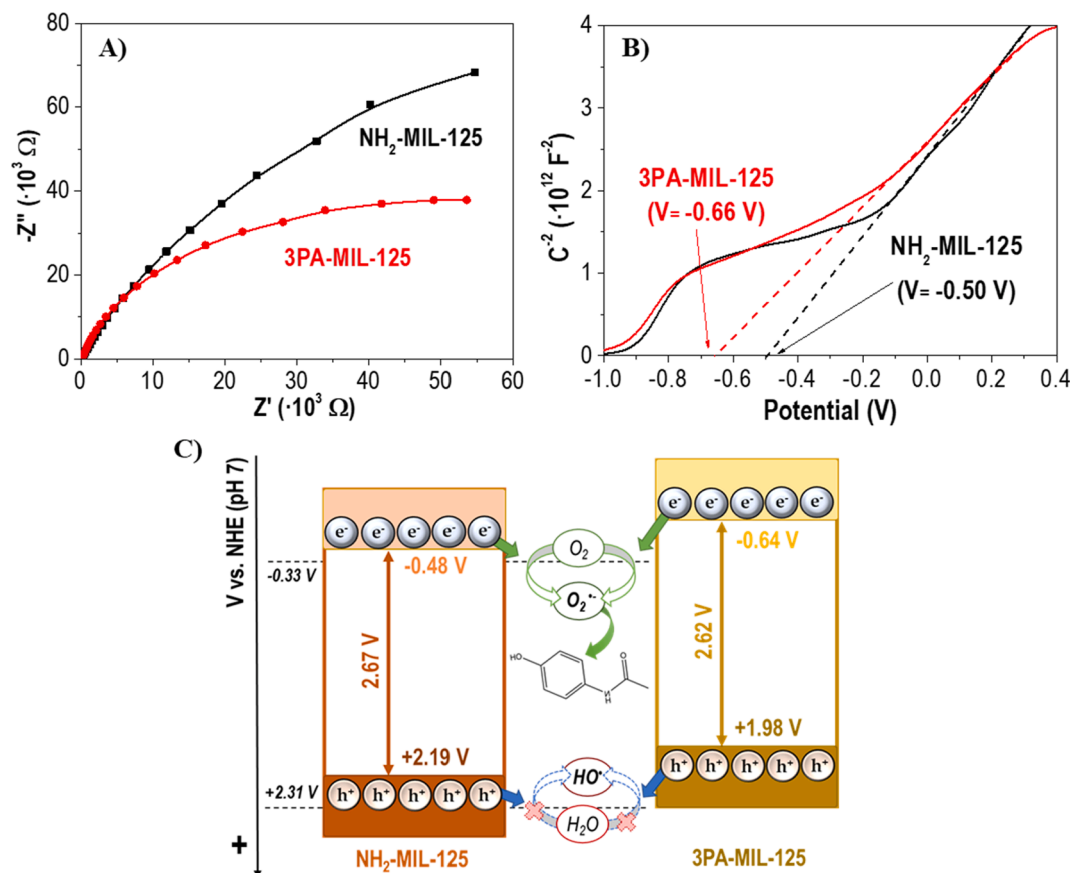


**Fig. 9.** (a) EIS Nyquist and (b) Mott-Schottky plots of  $\text{NH}_2\text{-MIL-125}$  and 3PA-MIL-125. (c) Proposed photocatalytic mechanism of ACE removal.

### 3. Results and discussion

#### 3.1. Characterization

The XRD diffractograms of all materials are depicted in Fig. 1. All grafted materials have very similar diffractograms to that of  $\text{NH}_2\text{-MIL-125}$  [32,35], characterized by intense peaks at  $6.8$ ,  $9.5$ , and  $11.6^\circ$  of  $2\theta$

assigned to the (101), (200), and (211) reflections, respectively, (COD-7211159.cif [48]). Thus, it can be confirmed that  $\text{NH}_2\text{-MIL-125}$  maintains its structural framework after grafting with the different heterocycles. Fig. 2 shows the solid  $^{13}\text{C}$  MAS NMR spectra of all synthesized materials. The peak at 180 ppm is characteristic of C atoms from the carboxylic group of the ligand bonded to the Ti-clusters, common to all synthesized materials (see chemical structure in Fig. S4) [49,50]. The

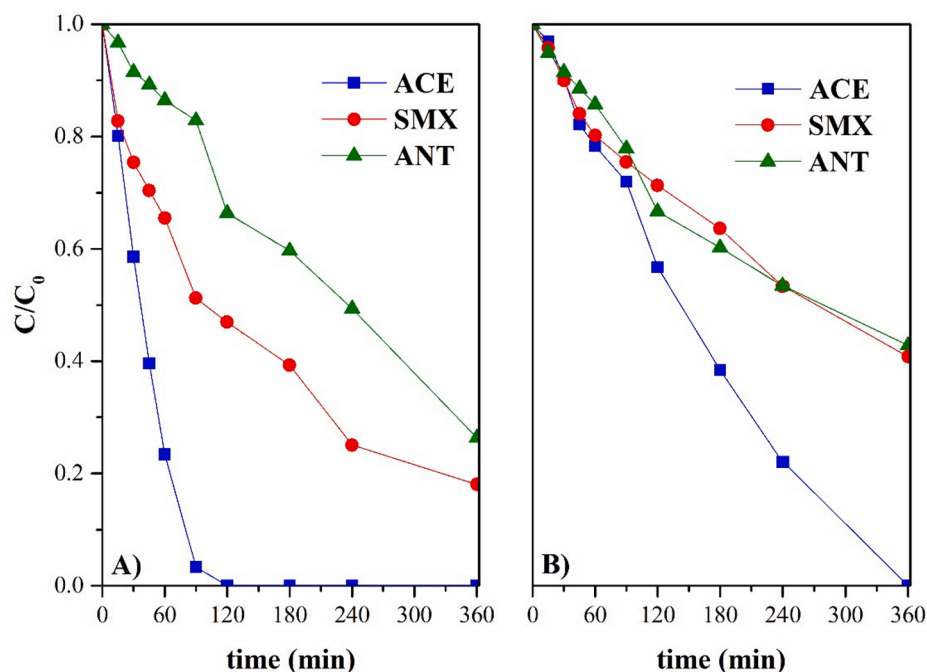


**Fig. 10.** Evolution of ACE, SMX and ANT upon reaction time with 3PA-MIL-125: A) individual experiments and B) mixture experiment ( $[ACE]_0 = 5 \text{ mg}\cdot\text{L}^{-1}$ ;  $[SMX]_0 = 5 \text{ mg}\cdot\text{L}^{-1}$ ;  $[ANT]_0 = 5 \text{ mg}\cdot\text{L}^{-1}$ ; Photocatalyst load =  $250 \text{ mg}\cdot\text{L}^{-1}$ ; Intensity =  $600 \text{ W}\cdot\text{m}^{-2}$ ).

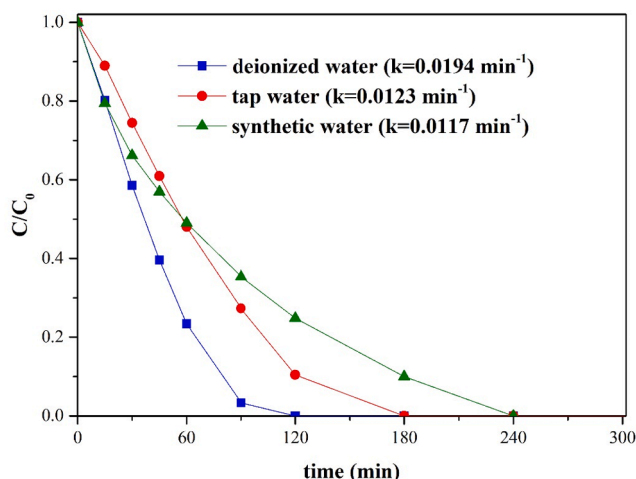


**Fig. 11.** Time-course of ACE concentration with 3PA-MIL-125 under solar irradiation in different water matrices.

resonance corresponding to carbon atoms bonded to the amine group of  $\text{NH}_2\text{-MIL-125}$ , i.e.  $\text{C-NH}_2$ , is visible at 150 ppm [49]. This signal suffers a broadening after grafting with the heterocycles, since some  $\text{C-NH}_2$  groups are transformed to  $\text{C-N}=\text{C}$  by a Schiff reaction (Fig. S2). The resonances of the quaternary aromatic carbon atoms appear in the range 140–130 ppm [49,50], which undergo significant modification after grafting due to the incorporation of pyridinic groups. This change is even more evident in the case of 2QUI since the ligand is grafted by the inclusion of a quinolinic group (Fig. S4). The signals observed at a lower chemical shift ( $\approx 120 \text{ ppm}$ ) are assigned to the carbon atoms bonded to a proton, i.e.  $-\text{CH}$  group [49,50]. Once again, grafting with heterocycles causes a signal broadening due to the addition of new  $-\text{CH}$  groups from the pyridine ring (2PA, 3PA, and 4PA), and quinoline ring on 2QUI-MIL-125. It should be mentioned that the spectra of the 2PA-, 3PA-, and 4PA-MIL-125 are very similar because the three heterocycles used are isomers. These results confirm the successful grafting of the ATA ligand by

a post-synthetic procedure in all cases under study, resulting in the chemical structures schematized in Fig. S4.

The porous texture parameters of all synthesized materials were determined from  $\text{N}_2$  adsorption-desorption isotherms at  $-196^\circ\text{C}$  (Fig. 3) and are summarized in Table 1. The isotherms can be classified as type I (IUPAC classification [51]) characteristic of microporous materials. All materials show high surface area values (between 911 and  $1141 \text{ m}^2\cdot\text{g}^{-1}$ ) due mainly to the contribution of micropores. Grafted materials showed a slightly lower amount of nitrogen adsorbed and, consequently, lower surface area values than the pristine  $\text{NH}_2\text{-MIL-125}$ , being this reduction more evident for 2QUI-MIL-125. This effect can be due to the larger size of the organic molecules anchored to the ligand that can partially block the porosity [38].

The optical properties of all synthesized materials were determined by UV-vis spectroscopy. Fig. 4 represents the absorbance spectra. All materials show the same absorption bands in the 200–300 nm range due to the presence of the Ti-oxo-clusters [52,53]. The band located at higher wavelengths is due to the linker absorption that shifts slightly from 390 to 400 nm after grafting with heterocycles. Thus, the grafted materials show some shift of absorption to the visible range, suggesting that the heterocycle molecules act as an antenna favouring light absorption [54]. The grafting process also showed an effect in the band gap values (Table 1), obtained from the Tauc plot (Fig. S5), whose values are slightly reduced after grafting. The morphology of all synthesized materials can be observed in the SEM images shown in Fig. 5. All samples describe thin and disk-like particles with a smooth surface similar to that of  $\text{NH}_2\text{-MIL-125}$  [52,55], with a mean size of 400–650 nm. Thus, the grafting post-treatment does not affect the particle morphology.

MOFs stability in water is a very important issue to consider in the practical use of these materials for water purification [56–59]. Following our previous work dealing with the  $\text{NH}_2\text{-MIL-125}$  stability [36], the amount of released ligand was determined by analyzing the filtrates after suspending the materials in an aqueous medium. The leachate percentage was determined by Eq. (4):

$$\text{Leachate}(\%) = \frac{C_{\text{ligand}}}{C_{\text{MOF}}} \times \frac{M_{\text{MOF}}}{6 \times M_{\text{ligand}}} \times 100 \quad (4)$$

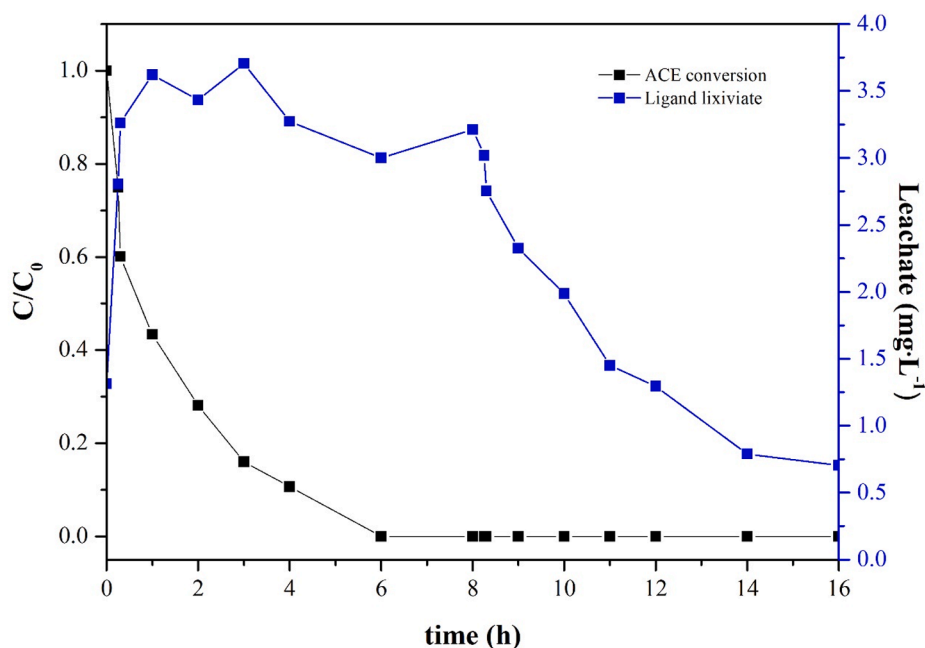


Fig. 12. Time-course of ACE and ligand leachate on stream in a continuous experiment with 3PA-MIL-125.

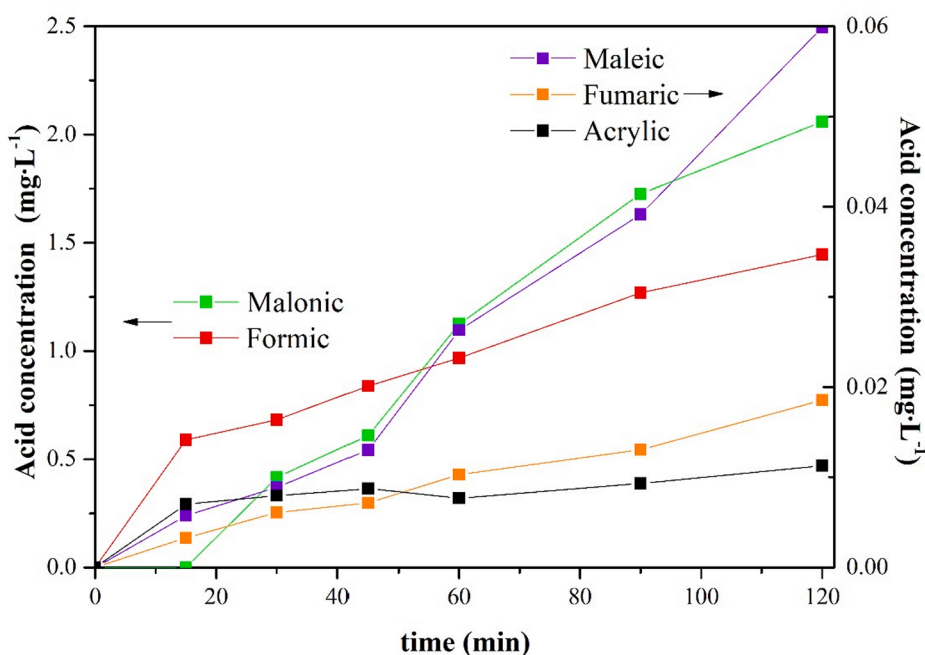


Fig. 13. Evolution of short-chain acids from the oxidation route of ACE ( $[ACE]_0 = 100 \text{ mg}\cdot\text{L}^{-1}$ ; Photocatalyst load =  $250 \text{ mg}\cdot\text{L}^{-1}$ ; Intensity =  $600 \text{ W}\cdot\text{m}^{-2}$ ).

where  $C_{\text{ligand}}$  is the ligand concentration detected in water ( $\text{mg}\cdot\text{L}^{-1}$ ), CMOF is the concentration of the MOF suspended in water, MMOF and  $M_{\text{ligand}}$  are the molecular weight values of the MOF and the ligand, respectively. Fig. 6 shows both the evolution in the concentration of the ligand detected and the percentage leached in relation to the total ligand content of the MOF. All grafted materials present lower ligand lixiviation than that of the bare  $\text{NH}_2\text{-MIL-125}$ , hence, it seems that the grafting improves the stability in water. In fact, ligand grafting is considered an approach to enhance the stability of MOFs in water, as it can lead to changes in surface hydrophobicity and steric size [60]. It should be noted that the low leaching could broaden the potential applications of these materials in aqueous media processes.

### 3.2. Photocatalytic performance assays

The photocatalytic performance of all materials herein synthesized was evaluated for ACE degradation under simulated solar light irradiation. Fig. 7 shows the evolution of ACE concentration with irradiation time after reaching the adsorption equilibrium in the dark. All grafted materials describe a better photocatalytic performance than the bare MOF, being 3PA-MIL-125 the most active, achieving almost total ACE degradation in 90 min. All degradation profiles were successfully fitted to a pseudo-first order kinetic reaction, being the kinetic constant values collected in Table 2. It is noteworthy that the kinetic constant of 3PA-MIL-125 is 2.4 times higher than that of the original  $\text{NH}_2\text{-MIL-125}$ .



These values have been compared with those already reported under the same reaction conditions with  $\text{NH}_2\text{-MIL-125}$  MOF with other modifications, i.e., Zr-doping [32] and Pt decoration [33]. It should be noted that the grafting of the ATA ligand with heterocycles promotes the photocatalytic reaction to a greater extent than those other modifications. This is most likely due to the aforementioned action of the heterocycle as an antenna favoring the ligand-to-metal charge transfer (LMCT) mechanism characteristic of MOFs [29,30]. Regarding the differences in photoactivity observed when using the different heterocyclic carboxaldehydes for the grafting, since the abovementioned properties were very similar, i.e. structure, porous properties and band gap, even the rate of electron-hole recombination was similar (shown in Fig. S6), the difference could be attributed to the steric arrangement of the heterocycle (schematized in Fig. S4).

To learn more about the reactive species involved in the ACE breakdown mechanism using 3PA-MIL-125, Fig. 8 represents the ACE evolution upon irradiation time in trapping experiments with different scavengers. KI had a negligible effect on the reaction, indicating that holes should not contribute to the process. The inhibitory effect of IPA was very low, suggesting a minor role of  $\text{HO}^\bullet$  radicals, and a similar effect was observed by the addition of  $\text{AgNO}_3$ , also suggesting a low contribution of the electrons. However, the incorporation of BQ suppressed remarkably the ACE degradation, indicating that  $\text{O}_2^\bullet$  radicals are the most likely reactive species in the photocatalytic process. This main contribution of  $\text{O}_2^\bullet$  radicals is in agreement with other works dealing with  $\text{NH}_2\text{-MIL-125}$  previously reported by our group [32–34].

Electrochemical characterization was also assessed to rationalize the likely causes of the better photocatalytic activity of 3PA-MIL-125 with respect to  $\text{NH}_2\text{-MIL-125}$ . In this sense, the resistance for surface charge transfer has been previously analyzed by EIS through the Nyquist plot [37,61]. As observed in Fig. 9a by the smaller arc radius of the semicircle, the higher performance of 3PA-MIL-125 can be attributed to a better interfacial charge transfer. Besides, Mott-Schottky plots were used to examine the bands alignment. From the intercept of the tangent lines with the potential axis in Fig. 9b and using Eq. (1), the flat band potentials ( $V_{\text{fb}}$ ) of 3PA-MIL-125 and  $\text{NH}_2\text{-MIL-125}$  were estimated to be  $-0.69$  and  $-0.53$  V, respectively. Following Eq. (2), the  $V_{\text{CB}}$  of both MOFs was determined to be  $-0.64$  and  $-0.48$  V, respectively, Eq. (3) was used to obtain the values of the  $V_{\text{VB}}$  considering the  $E_g$  of each photocatalyst (Table 1). The  $V_{\text{CB}}$  value estimated in this study for  $\text{NH}_2\text{-MIL-125}$  lies within the range of those reported for this MOF in the literature ( $-0.32 < V_{\text{CB}} < -0.87$  V [62,63]). Fig. 9c schematizes a tentative band structure for both MOFs. Grafting the  $\text{NH}_2\text{-MIL-125}$  with 3PA heterocyclic carboxaldehyde resulted in a slight reduction of the band gap (Table 1) and a displacement of the position of both CB and VB. This displacement favors and supports the generation of the  $\text{O}_2^\bullet$  described above. The formation of this radical through the dissolved oxygen reduction ( $-0.33$  V vs NHE at pH 7 [64]) is energetically favored, even more than on the  $\text{NH}_2\text{-MIL-125}$ , while the generation of  $\text{HO}^\bullet$  after water oxidation ( $+2.31$  V vs NHE at pH 7 [65]) is energetically prevented due to the position of the valence band.

Since 3PA-MIL-125 proved its promising photocatalytic performance in the conversion of ACE, the degradation of other emerging contaminants, i.e. SMX and ANT, was also tested. Fig. 10A shows the evolution of SMX and ANT concentration with irradiation time in individual tests (in the presence of only one of the pollutants). The photocatalytic degradations of SMX and ANT were slower than that of ACE, revealing the more refractory character of these compounds. This issue can be associated with their chemical structure (shown in Fig. S7). Unlike ACE, which has an aromatic ring easier to open [66,67], SMX has a second heterocycle, i.e. a sulfonamide group, that makes its degradation more difficult [68]. Something similar occurs with ANT, whose pyrazolone group makes it more refractory to oxidation [17]. The removal of the three pharmaceuticals was also evaluated in a mixture (Fig. 10B). 3PA-MIL-125 was able to degrade the three of them simultaneously, although the conversion rates achieved were lower than those obtained when they

are degraded separately. This difference can be ascribed to several factors: i) the competition among ACE, SMX, and ANT molecules for the photocatalyst surface, ii) the oxidative species have a more organic matter to degrade, and/or iii) the formation of reaction by-products that can interfere in the degradation process. Remarkably, no works have been previously reported dealing with the photodegradation of these contaminants with  $\text{NH}_2\text{-MIL-125}$  grafted with 3-pyridinecarboxaldehyde.

The effect of the water matrix was also assessed for ACE removal with 3PA-MIL-125. Fig. 11 depicted the photocatalytic degradation of ACE in deionized water, tap water, and synthetic water. Total conversion of ACE was achieved in all cases, but the reaction rate is reduced when tap water is used and even more when using synthetic water. This decrease is due to the presence of inorganic ions (such as  $\text{Cl}^-$ ,  $\text{NO}_3^-$ ,  $\text{SO}_4^{2-}$  or  $\text{HCO}_3^-$ ) capable of trapping the photogenerated charges and radicals. This behavior is in agreement with previous results dealing with other photocatalysts based on MOFs [33].

Batch systems present a huge disadvantage since it is necessary to separate the photocatalyst from the treated water [46–48]. Thus, the photocatalytic performance of 3PA-MIL-125 was evaluated in a 16 h continuous flow system (set-up schematized in Fig. S3). Fig. 12 shows the time-course of ACE and leached ligand on stream during this test. Once the steady-state was reached (about 6 h), the photocatalytic performance remained constant, achieving a total conversion of ACE, and thus demonstrating the stability of 3PA-MIL-125. Ligand leaching was also monitored, and a low concentration of leachate was observed ( $<4 \text{ mg}\cdot\text{L}^{-1}$ ), which continuously decreases from 8 h of reaction and practically disappeared after 16 h on stream. After reaction, the photocatalyst was recovered and characterized to analyze its structural stability. XRD and  $\text{N}_2$  adsorption-desorption results were very similar to those described above for the neat 3PA-MIL-125 (Fig. S8). Only a slight reduction of the surface area was detected, which may be associated with the deposition of by-products, which can slightly block the porous network. Thus, 3PA-MIL-125 appears as an active and stable photocatalyst to remove emerging contaminants from water under solar irradiation in a continuous flow system.

The acetaminophen degradation pathway has been previously reported by our research group [15,17,33]. We proposed several reaction routes involving ring-opening, coupling, hydroxylation, acetamide loss, and oxidation processes. Short-chain acids were detected as succinic, malonic, formic, and acetic acids. In the current study, up to five different carboxylic acids, namely maleic, malonic, formic, fumaric, and acrylic acids, were identified from the photocatalytic degradation of ACE by 3PA-MIL-125, as detailed in Fig. 13. Malonic and formic acids are continuously formed along with the experiment, while malonic acid appeared after 30 min under solar light irradiation. Similar behaviour was shown for maleic, fumaric, and acrylic acids, although their concentrations were lower. It seems that the grafted MOF allows the transformation of ACE giving rise to compounds of lower complexity.

#### 4. Conclusions

The photocatalytic performance of  $\text{NH}_2\text{-MIL-125}$  was improved by grafting the amine ligand with heterocycles that act as an antenna for visible light absorption. 3PA-MIL-125 exhibited the best performance in acetaminophen degradation due to its high specific surface area and microporosity, slightly lower band gap, improved light absorption, better interfacial charge transference, and reduced electron-hole recombination. Experiments with scavengers lead to the conclusion that superoxide radicals play a major role in the photodegradation of acetaminophen, although electrons and hydroxyl radicals are also partly involved. The inorganic ions commonly found in water reduced the acetaminophen photodegradation. 3PA-MIL-125 was able to remove other emerging contaminants, i.e. sulfamethoxazole and antipyrine, and even a mixture of them, although the reaction rate depends on the nature of the target compound. In a continuous flow regime, total

degradation of acetaminophen was reached after 6 h and then maintained for the rest of the 16 h experiment. The current results revealed the stability and activity of the grafted-NH<sub>2</sub>-MIL-125 with 3-pyridine-carboxaldehyde photocatalyst for the remediation of pharmaceuticals in water on stream under solar irradiation.

## Declaration of Competing Interest

The authors declare that they have no known competing financial interests or personal relationships that could have appeared to influence the work reported in this paper.

## Acknowledgement

This research was funded by State Research Agency (PID2019-106186RB-I00/AEI/10.13039/501100011033). V. Muelas-Ramos thanks to MCIU for BES-2017-082613 grant. M. Peñas-Garzón is indebted to Spanish MECO (FPU16/00576 grant). The authors thank the Research Support Services of the University of Extremadura (SAIUEX) for SEM images.

## Appendix A. Supplementary material

Supplementary data to this article can be found online at <https://doi.org/10.1016/j.seppur.2022.121442>.

## References

- [1] J. Rivera-Utrilla, M. Sánchez-Polo, M.Á. Ferro-García, G. Prados-Joya, R. Ocampo-Pérez, Pharmaceuticals as emerging contaminants and their removal from water. A review, *Chemosphere* 93 (2013) 1268–1287, <https://doi.org/10.1016/j.chemosphere.2013.07.059>.
- [2] C. Regmi, E. Maya-Flores, S.W. Lee, V. Rodríguez-González, Cerium-doped  $\beta$ -Ni(OH)<sub>2</sub> hexagon nanosheets: an effective photocatalyst for the degradation of the emerging water pollutant, naproxen, *Nanotechnology* 29 (2018) 375603, <https://doi.org/10.1088/1361-6528/AACE14>.
- [3] M.Q. Cai, R. Wang, L. Feng, L.Q. Zhang, Determination of selected pharmaceuticals in tap water and drinking water treatment plant by high-performance liquid chromatography-triple quadrupole mass spectrometer in Beijing, China, *Environ. Sci. Pollut. Res.* 22 (2014) 1854–1867, <https://doi.org/10.1007/S11356-014-3473-8>.
- [4] M. Papageorgiou, C. Kosma, D. Lambropoulou, Seasonal occurrence, removal, mass loading and environmental risk assessment of 55 pharmaceuticals and personal care products in a municipal wastewater treatment plant in Central Greece, *Sci. Total Environ.* 543 (2016) 547–569, <https://doi.org/10.1016/j.scitotenv.2015.11.047>.
- [5] T. Deblonde, C. Cossu-Leguille, P. Hartemann, Emerging pollutants in wastewater: A review of the literature, *Int. J. Hyg. Environ. Health* 214 (2011) 442–448, <https://doi.org/10.1016/j.ijheh.2011.08.002>.
- [6] K. Hider-Mlynarz, P. Cavalieri, P. Maisson, Trends in analgesic consumption in France over the last 10 years and comparison of patterns across Europe, *Br. J. Clin. Pharmacol.* 84 (2018) 1324–1334, <https://doi.org/10.1111/BCP.13564>.
- [7] E. Yoon, A. Babar, M. Choudhary, M. Kutner, N. Pyrsopoulos, Acetaminophen-induced hepatotoxicity: a comprehensive update, *J. Clin. Transl. Hepatol.* 4 (2016) 131, <https://doi.org/10.14218/JCTH.2015.00052>.
- [8] R. Taylor, J.V. Pergolizzi, Acetaminophen (paracetamol): Properties, clinical uses, and adverse effects, in: *Pharmacol. Res. Saf. Test. Regul.*, 2012: pp. 1–24.
- [9] S. Fekadu, E. Alemayehu, R. Dewil, B. Van der Bruggen, Pharmaceuticals in freshwater aquatic environments: A comparison of the African and European challenge, *Sci. Total Environ.* 654 (2019) 324–337, <https://doi.org/10.1016/j.scitotenv.2018.11.072>.
- [10] M.R. Boleda, M.T. Galceran, F. Ventura, Validation and uncertainty estimation of a multiresidue method for pharmaceuticals in surface and treated waters by liquid chromatography-tandem mass spectrometry, *J. Chromatogr. A* 1286 (2013) 146–158, <https://doi.org/10.1016/j.chroma.2013.02.077>.
- [11] K.O. K'oreje, L. Vergeynst, D. Ombaka, P. De Wispelaere, M. Okoth, H. Van Langenhove, K. Demeestere, Occurrence patterns of pharmaceutical residues in wastewater, surface water and groundwater of Nairobi and Kisumu city, Kenya, *Chemosphere* 149 (2016) 238–244, <https://doi.org/10.1016/j.chemosphere.2016.01.095>.
- [12] J. Wang, S. Wang, Activation of persulfate (PS) and peroxydisulfate (PMS) and application for the degradation of emerging contaminants, *Chem. Eng. J.* 334 (2018) 1502–1517, <https://doi.org/10.1016/j.cej.2017.11.059>.
- [13] Y. Deng, R. Zhao, Advanced oxidation processes (AOPs) in wastewater treatment, *Curr. Pollut. Reports* 1 (2015) 167–176, <https://doi.org/10.1007/s40726-015-0015-z>.
- [14] A.R. Ribeiro, O.C. Nunes, M.F.R. Pereira, A.M.T. Silva, An overview on the advanced oxidation processes applied for the treatment of water pollutants defined in the recently launched Directive 2013/39/EU, *Environ. Int.* 75 (2015) 33–51, <https://doi.org/10.1016/j.envint.2014.10.027>.
- [15] Y.L. Wang, S. Zhang, Y.F. Zhao, J. Bedia, J.J. Rodriguez, C. Belver, UiO-66-based metal organic frameworks for the photodegradation of acetaminophen under simulated solar irradiation, *J. Environ. Chem. Eng.* 9 (2021) 106087, <https://doi.org/10.1016/J.JECE.2021.106087>.
- [16] A. Gómez-Avilés, M. Peñas-Garzón, J. Bedia, J.J. Rodriguez, C. Belver, C-modified TiO<sub>2</sub> using lignin as carbon precursor for the solar photocatalytic degradation of acetaminophen, *Chem. Eng. J.* 358 (2019) 1574–1582, <https://doi.org/10.1016/j.cej.2018.10.154>.
- [17] M. Peñas-Garzón, A. Gómez-Avilés, C. Belver, J.J. Rodriguez, J. Bedia, Degradation pathways of emerging contaminants using TiO<sub>2</sub>-activated carbon heterostructures in aqueous solution under simulated solar light, *Chem. Eng. J.* 392 (2020) 124867, <https://doi.org/10.1016/J.CEJ.2020.124867>.
- [18] M. Akkari, P. Aranda, C. Belver, J. Bedia, A. Ben Haj Amara, E. Ruiz-Hitzky, ZnO/sepiolite heterostructured materials for solar photocatalytic degradation of pharmaceuticals in wastewater, *Appl. Clay Sci.* 156 (2018) 104–109, <https://doi.org/10.1016/j.clay.2018.01.021>.
- [19] H. Ji, W. Liu, F. Sun, T. Huang, L. Chen, Y. Liu, J. Qi, C. Xie, D. Zhao, Experimental evidences and theoretical calculations on phenanthrene degradation in a solar-light-driven photocatalysis system using silica aerogel supported TiO<sub>2</sub> nanoparticles: Insights into reactive sites and energy evolution, *Chem. Eng. J.* 419 (2021), 129605, <https://doi.org/10.1016/J.CEJ.2021.129605>.
- [20] N. Miranda-García, S. Suárez, B. Sánchez, J.M. Coronado, S. Malato, M. I. Maldonado, Photocatalytic degradation of emerging contaminants in municipal wastewater treatment plant effluents using immobilized TiO<sub>2</sub> in a solar pilot plant, *Appl. Catal. B Environ.* 103 (2011) 294–301, <https://doi.org/10.1016/j.apcatb.2011.01.030>.
- [21] A. Petala, D. Spyrou, Z. Frontistis, D. Mantzavinos, D.I. Kondarides, Immobilized Ag<sub>3</sub>PO<sub>4</sub> photocatalyst for micro-pollutants removal in a continuous flow annular photoreactor, *Catal. Today* 328 (2019) 223–229, <https://doi.org/10.1016/j.cattod.2018.10.062>.
- [22] P. Ding, H. Ji, P. Li, Q. Liu, Y. Wu, M. Guo, Z. Zhou, S. Gao, W. Xu, W. Liu, Q. Wang, S. Chen, Visible-light degradation of antibiotics catalyzed by titania/zirconia/graphitic carbon nitride ternary nanocomposites: a combined experimental and theoretical study, *Appl. Catal. B Environ.* 300 (2022), 120633, <https://doi.org/10.1016/J.APCATB.2021.120633>.
- [23] X. Li, J. Xie, C. Jiang, J. Yu, P. Zhang, Review on design and evaluation of environmental photocatalysts, *Front. Environ. Sci. Eng.* 12 (2018) 1–32, <https://doi.org/10.1007/S11783-018-1076-1>.
- [24] J. Wen, J. Xie, X. Chen, X. Li, A review on g-C<sub>3</sub>N<sub>4</sub>-based photocatalysts, *Appl. Surf. Sci.* 391 (2017) 72–123, <https://doi.org/10.1016/j.apsusc.2016.07.030>.
- [25] C. Belver, J. Bedia, A. Gómez-Avilés, M. Peñas-Garzón, J.J. Rodriguez, Semiconductor Photocatalysis for Water Purification, in: *Nanoscale Mater. Water Purif.*, Elsevier, 2018: pp. 581–651. doi:10.1016/B978-0-12-813926-4.00028-8.
- [26] G. Zahn, H.A. Schulze, J. Lippke, S. König, U. Sazama, M. Fröba, P. Behrens, A water-born Zr-based porous coordination polymer: Modulated synthesis of Zr-fumarate MOF, *Microporous Mesoporous Mater.* 203 (2015) 186–194, <https://doi.org/10.1016/J.MICROMESO.2014.10.034>.
- [27] J. Bedia, V. Muelas-Ramos, M. Peñas-Garzón, A. Gómez-Avilés, J. Rodríguez, C. Belver, A review on the synthesis and characterization of metal organic frameworks for photocatalytic water purification, *Catalysts* 9 (2019) 52, <https://doi.org/10.3390/catal9010052>.
- [28] L. Zeng, X. Guo, C. He, C. Duan, Metal-Organic Frameworks: Versatile materials for heterogeneous photocatalysis, *ACS Catal.* 6 (2016) 7935–7947, <https://doi.org/10.1021/acscatal.6b02228>.
- [29] M. Alvaro, E. Carbonell, B. Ferrer, F. LlabrésXamena, H. García, Semiconductor behavior of a metal-organic framework (MOF), *Chem. A Eur. J.* 13 (18) (2007) 5106–5112, <https://doi.org/10.1002/chem.200601003>.
- [30] J. Qiu, X. Zhang, Y. Feng, X. Zhang, H. Wang, J. Yao, Modified metal-organic frameworks as photocatalysts, *Appl. Catal. B Environ.* 231 (2018) 317–342, <https://doi.org/10.1016/j.apcatb.2018.03.039>.
- [31] Z.U. Zango, K. Jumbri, N.S. Sambudi, A. Ramli, N.H.H.A. Bakar, B. Saad, M.N. H. Rozaini, H.A. Isiyaka, A.H. Jagaba, O. Aldaghri, A. Sulieman, A critical review on metal-organic frameworks and their composites as advanced materials for adsorption and photocatalytic degradation of emerging organic pollutants from wastewater, *Polymers (Basel)* 12 (2020) 2648, <https://doi.org/10.3390/POLYM12112648>.
- [32] A. Gómez-Avilés, M. Peñas-Garzón, J. Bedia, D.D. Dionysiou, J.J. Rodríguez, C. Belver, Mixed Ti-Zr metal-organic-frameworks for the photodegradation of acetaminophen under solar irradiation, *Appl. Catal. B Environ.* 253 (2019) 253–262, <https://doi.org/10.1016/j.apcatb.2019.04.040>.
- [33] V. Muelas-Ramos, C. Belver, J.J. Rodriguez, J. Bedia, Synthesis of noble metal-decorated NH<sub>2</sub>-MIL-125 titanium MOF for the photocatalytic degradation of acetaminophen under solar irradiation, *Sep. Purif. Technol.* 272 (2021), 118896, <https://doi.org/10.1016/j.seppur.2021.118896>.
- [34] V. Muelas-Ramos, M.J. Sampaio, C.G. Silva, J. Bedia, J.J. Rodriguez, J.L. Faria, C. Belver, Degradation of diclofenac in water under LED irradiation using combined g-C<sub>3</sub>N<sub>4</sub>/NH<sub>2</sub>-MIL-125 photocatalysts, *J. Hazard. Mater.* 416 (2021), 126199, <https://doi.org/10.1016/J.JHAZMAT.2021.126199>.
- [35] S.R. Zhu, P.F. Liu, M.K. Wu, W.N. Zhao, G.C. Li, K. Tao, F.Y. Yi, L. Han, Enhanced photocatalytic performance of BiOBr/NH<sub>2</sub>-MIL-125(Ti) composite for dye degradation under visible light, *Dalt. Trans.* 45 (2016) 17521–17529, <https://doi.org/10.1039/C6DT02912D>.

- [36] A. Gómez-Avilés, V. Muelas-Ramos, J. Bedia, J.J. Rodríguez, C. Belver, Thermal Post-Treatments to Enhance the Water Stability of  $\text{NH}_2\text{-MIL-125(Ti)}$ , *Catalysts*. 10 (2020) 603, <https://doi.org/10.3390/catal10060603>.
- [37] R.R. Solís, A. Gómez-Avilés, C. Belver, J.J. Rodríguez, J. Bedia, Microwave-assisted synthesis of  $\text{NH}_2\text{-MIL-125(Ti)}$  for the solar photocatalytic degradation of aqueous emerging pollutants in batch and continuous tests, *J. Environ. Chem. Eng.* 9 (5) (2021) 106230, <https://doi.org/10.1016/j.jece.2021.106230>.
- [38] Z. Wu, X. Huang, H. Zheng, P. Wang, G. Hai, W. Dong, G. Wang, Aromatic heterocycle-grafted  $\text{NH}_2\text{-MIL-125(Ti)}$  via conjugated linker with enhanced photocatalytic activity for selective oxidation of alcohols under visible light, *Appl. Catal. B Environ.* 224 (2018) 479–487, <https://doi.org/10.1016/j.apcatb.2017.10.034>.
- [39] H.M.A. Hassan, M.A. Betiha, S.K. Mohamed, E.A. El-Sharkawy, E.A. Ahmed, Salen-Zr(IV) complex grafted into amine-tagged MIL-101(Cr) as a robust multifunctional catalyst for biodiesel production and organic transformation reactions, *Appl. Surf. Sci.* 412 (2017) 394–404, <https://doi.org/10.1016/j.apsusc.2017.03.247>.
- [40] O.A.M. Ali, S.M. El-Medani, D.A. Ahmed, D.A. Nassar, Synthesis, characterization, fluorescence and catalytic activity of some new complexes of unsymmetrical Schiff base of 2-pyridinecarboxaldehyde with 2,6-diaminopyridine, *Spectrochim. Acta - Part A Mol. Biomol. Spectrosc.* 144 (2015) 99–106, <https://doi.org/10.1016/j.saa.2015.02.078>.
- [41] S.Y. Bunting, D.J. Lapworth, E.J. Crane, J. Grima-Olmedo, A. Koroša, A. Kuczyńska, N. Mali, L. Rosenqvist, M.E. van Vliet, A. Togola, B. Lopez, Emerging organic compounds in European groundwater, *Environ. Pollut.* 269 (2021) 115945, <https://doi.org/10.1016/j.envpol.2020.115945>.
- [42] K.S. Walton, R.Q. Snurr, Applicability of the BET method for determining surface areas of microporous metal-organic frameworks, *J. Am. Chem. Soc.* 129 (2007) 8552–8556, <https://doi.org/10.1021/ja071174k>.
- [43] A.J. Howarth, A.W. Peters, N.A. Vermeulen, T.C. Wang, J.T. Hupp, O.K. Farha, Best practices for the synthesis, activation, and characterization of metal-organic frameworks, *Chem. Mater.* 29 (2017) 26–39, <https://doi.org/10.1021/acs.chemmater.6b02626>.
- [44] J. Tauc, Absorption edge and internal electric fields in amorphous semiconductors, *Mater. Res. Bull.* 5 (1970) 721–729, [https://doi.org/10.1016/0025-5408\(70\)90112-1](https://doi.org/10.1016/0025-5408(70)90112-1).
- [45] S. Kampouri, C.P. Ireland, B. Valizadeh, E. Oveisi, P.A. Schouwink, M. Mensi, K. C. Stylianou, Mixed-Phase MOF-Derived titanium dioxide for photocatalytic hydrogen evolution: the impact of the templated morphology, *ACS Appl. Energy Mater.* 1 (2018) 6541–6548, <https://doi.org/10.1021/acs.aem.8b01445>.
- [46] C. Baumanis, D.W. Bahnemann,  $\text{TiO}_2$  thin film electrodes: Correlation between photocatalytic activity and electrochemical properties, *J. Phys. Chem. C* 112 (2008) 19097–19101, <https://doi.org/10.1021/jp807655a>.
- [47] T. Giannakopoulou, I. Papailias, N. Todorova, N. Boukos, Y. Liu, J. Yu, C. Trapalis, Tailoring the energy band gap and edges' potentials of  $\text{g-C}_3\text{N}_4/\text{TiO}_2$  composite photocatalysts for  $\text{NO}_x$  removal, *Chem. Eng. J.* 310 (2017) 571–580, <https://doi.org/10.1016/j.cej.2015.12.102>.
- [48] A.P. Smalley, D.G. Reid, J.C. Tan, G.O. Lloyd, Alternative synthetic methodology for amide formation in the post-synthetic modification of  $\text{Ti-MIL125-NH}_2$ , *CrystEngComm*. 15 (2013) 9368, <https://doi.org/10.1039/c3ce41332b>.
- [49] A. Rossini, A.J. Zagdoun, A. Lelli, M. Canivet, J. Aguado, S. Ouari, O. Tordo, P. Rosay, M. Maas, W.E. Copéret, C. Farrusseng, D. Emsley, L. Lesage, Dynamic nuclear polarization enhanced solid-state NMR spectroscopy of functionalized metal-organic frameworks, *Angew. Chem. Int. Ed. Engl.* 51 (2012) 123–127, <https://doi.org/10.1002/anie.201106030>.
- [50] S. Devautour-Vinot, G. Maurin, C. Serre, P. Horcajada, D. Paula da Cunha, V. Guillerm, E. de Souza Costa, F. Taulelle, C. Martineau, Structure and Dynamics of the Functionalized MOF Type  $\text{UiO-66(Zr)}$ : NMR and Dielectric Relaxation Spectroscopies Coupled with DFT Calculations, *Chem. Mater.* 24 (11) (2012) 2168–2177, <https://doi.org/10.1021/CM300863C>.
- [51] K. Sing, Reporting physisorption data for gas/solid systems, *Pure Appl. Chem.* 54 (1982) 2201–2218, <https://doi.org/10.1351/pac198254112201>.
- [52] Y.H. Fan, S.W. Zhang, S. Bin Qin, X.S. Li, S.H. Qi, An enhanced adsorption of organic dyes onto  $\text{NH}_2$  functionalization titanium-based metal-organic frameworks and the mechanism investigation, *Microporous Mesoporous Mater.* 263 (2018) 120–127, [doi:10.1016/j.micromeso.2017.12.016](https://doi.org/10.1016/j.micromeso.2017.12.016).
- [53] H. Huang, X.S. Wang, D. Philo, F. Ichihara, H. Song, Y. Li, D. Li, T. Qiu, S. Wang, J. Ye, Toward visible-light-assisted photocatalytic nitrogen fixation: A titanium metal organic framework with functionalized ligands, *Appl. Catal. B Environ.* 267 (2020), 118686, <https://doi.org/10.1016/j.apcatb.2020.118686>.
- [54] A. Dhakshinamoorthy, Z. Li, H. Garcia, Catalysis and photocatalysis by metal organic frameworks, *Chem. Soc. Rev.* 47 (2018) 8134–8172, <https://doi.org/10.1039/c8cs00256h>.
- [55] H. Wang, X. Yuan, Y. Wu, G. Zeng, X. Chen, L. Leng, Z. Wu, L. Jiang, H. Li, Facile synthesis of amino-functionalized titanium metal-organic frameworks and their superior visible-light photocatalytic activity for  $\text{Cr(VI)}$  reduction, *J. Hazard. Mater.* 286 (2015) 187–194, <https://doi.org/10.1016/j.jhazmat.2014.11.039>.
- [56] G. Wen, Z.G. Guo, Facile modification of  $\text{NH}_2\text{-MIL-125(Ti)}$  to enhance water stability for efficient adsorptive removal of crystal violet from aqueous solution, *Colloids Surfaces A Physicochem. Eng. Asp.* 541 (2018) 58–67, <https://doi.org/10.1016/j.colsurfa.2018.01.011>.
- [57] X. Qian, B. Yadian, R. Wu, Y. Long, K. Zhou, B. Zhu, Y. Huang, Structure stability of metal-organic framework MIL-53 (Al) in aqueous solutions, *Int. J. Hydrogen Energy*. 38 (2013) 16710–16715, <https://doi.org/10.1016/j.ijhydene.2013.07.054>.
- [58] K.A. Cychosz, A.J. Matzger, Water stability of microporous coordination polymers and the adsorption of pharmaceuticals from water, *Langmuir*. 26 (2010) 17198–17202, <https://doi.org/10.1021/la103234u>.
- [59] K.S. Park, Z. Ni, A.P. Côté, J.Y. Choi, R. Huang, F.J. Uribe-Romo, H.K. Chae, M. O'Keeffe, O.M. Yaghi, Exceptional chemical and thermal stability of zeolitic imidazolate frameworks, *Proc. Natl. Acad. Sci. U. S. A.* 103 (2006) 10186–10191, <https://doi.org/10.1073/pnas.0602439103>.
- [60] B. Liu, K. Vikrant, K.-H. Kim, V. Kumar, S.K. Kailasa, Critical role of water stability in metal-organic frameworks and advanced modification strategies for the extension of their applicability, *Environ. Sci. Nano* 7 (2020) 1319–1347, <https://doi.org/10.1039/C9EN01321K>.
- [61] H. Diarmand-Khalilabad, A. Habibi-Yangjeh, D. Seifzadeh, S. Asadzadeh-Khaneghah, E. Vesali-Kermani,  $\text{g-C}_3\text{N}_4$  nanosheets decorated with carbon dots and  $\text{CdS}$  nanoparticles: Novel nanocomposites with excellent nitrogen photofixation ability under simulated solar irradiation, *Ceram. Int.* 45 (2019) 2542–2555, <https://doi.org/10.1016/j.ceramint.2018.10.185>.
- [62] S. Luo, C. Zhang, X. Liu, Y. Li, L. Tang, M. Fu, S. Wang, J. Wu, M. Xu, X. Wang, Y. He, Protonated  $\text{NH}_2\text{-MIL-125}$  via  $\text{HCl}$  vapor to introduce the moiety with charge and ample hydrogen as a novel bifunctional photocatalyst: Enhanced photocatalytic  $\text{H}_2$  production and  $\text{NO}$  purification, *Chem. Eng. J.* 432 (2022), 134244, <https://doi.org/10.1016/j.cej.2021.134244>.
- [63] Y. Du, L. Zhao, H. Chen, Z. Huang, X. He, W. Fang, W. Li, F. Zhang, G. Wang, Synthesis and enhanced visible light-induced photocatalytic activity of a hierarchical porous biomorphic  $\text{N/Zn-TiO}_2/\text{NH}_2\text{-MIL-125}$  photocatalyst, *J. Mater. Sci. Mater. Electron.* 29 (2018) 20356–20366, <https://doi.org/10.1007/s10854-018-0171-1>.
- [64] X. Li, J. Yu, M. Jaroniec, Hierarchical photocatalysts, *Chem. Soc. Rev.* 45 (2016) 2603–2636, <https://doi.org/10.1039/c5cs00838g>.
- [65] W.H. Koppenol, D.M. Stanbury, P.L. Bounds, Electrode potentials of partially reduced oxygen species, from dioxygen to water, *Free Radic. Biol. Med.* 49 (2010) 317–322, <https://doi.org/10.1016/j.freeradbiomed.2010.04.011>.
- [66] R. Andreozzi, V. Caprio, R. Marotta, D. Vogna, Paracetamol oxidation from aqueous solutions by means of ozonation and  $\text{H}_2\text{O}_2/\text{UV}$  system, *Water Res.* 37 (2003) 993–1004, [https://doi.org/10.1016/S0043-1354\(02\)00460-8](https://doi.org/10.1016/S0043-1354(02)00460-8).
- [67] A.M. Abdel-Wahab, A.S. Al-Shirbini, O. Mohamed, O. Nasr, Photocatalytic degradation of paracetamol over magnetic flower-like  $\text{TiO}_2/\text{Fe}_2\text{O}_3$  core-shell nanostructures, *J. Photochem. Photobiol. A Chem.* 347 (2017) 186–198, <https://doi.org/10.1016/j.jphotochem.2017.07.030>.
- [68] Y. Song, J. Tian, S. Gao, P. Shao, J. Qi, F. Cui, Photodegradation of sulfonamides by  $\text{g-C}_3\text{N}_4$  under visible light irradiation: Effectiveness, mechanism and pathways, *Appl. Catal. B Environ.* 210 (2017) 88–96, <https://doi.org/10.1016/j.apcatb.2017.03.059>.